Human Molecular Genetics, 2011, Vol. 20, No. 7 **1411–1423**
doi:10.1093/hmg/ddr022
Advance Access published on January 18, 2011

Cone photoreceptors are the main targets for gene therapy of NPHP5 (IQCB1) or NPHP6 (CEP290) blindness: generation of an all-cone Nphp6 hypomorph mouse that mimics the human retinal ciliopathy

Artur V. Cideciyan[1,*], Rivka A. Rachel[2], Tomas S. Aleman[1], Malgorzata Swider[1], Sharon B. Schwartz[1], Alexander Sumaroka[1], Alejandro J. Roman[1], Edwin M. Stone[3,4], Samuel G. Jacobson[1] and Anand Swaroop[2]

[1]Department of Ophthalmology, Scheie Eye Institute, University of Pennsylvania, Philadelphia, PA, USA, [2]Neurobiology–Neurodegeneration and Repair Laboratory, National Eye Institute, National Institutes of Health, Bethesda, MD, USA and [3]Howard Hughes Medical Institute and [4]Department of Ophthalmology, University of Iowa Carver College of Medicine, Iowa City, IA, USA

Received November 1, 2010; Revised December 22, 2010; Accepted January 14, 2011

Leber congenital amaurosis (LCA), a severe autosomal recessive childhood blindness, is caused by mutations in at least 15 genes. The most common molecular form is a ciliopathy due to *NPHP6* (*CEP290*) mutations and subjects have profound loss of vision. A similarly severe phenotype occurs in the related ciliopathy *NPHP5 (IQCB1)*-LCA. Recent success of retinal gene therapy in one form of LCA prompted the question whether we know enough about human *NPHP5* and *NPHP6* disease to plan such treatment. We determined that there was early-onset rapid degeneration of rod photoreceptors in young subjects with these ciliopathies. Rod outer segment (OS) lamination, when detectable, was disorganized. Retinal pigment epithelium lipofuscin accumulation indicated that rods had existed in the past in most subjects. In contrast to early rod losses, the all-cone human fovea in *NPHP5*- and *NPHP6*-LCA of all ages retained cone nuclei, albeit with abnormal inner segments and OS. The *rd16* mouse, carrying a hypomorphic *Nphp6* allele, was a good model of the rod-dominant human extra-foveal retina. *Rd16* mice showed normal genesis of photoreceptors, including the formation of cilia, followed by abnormal elaboration of OS and rapid degeneration. To produce a model of the all-cone human fovea in *NPHP6*-LCA, we generated *rd16;Nrl*$^{-/-}$ double-mutant mice. They showed substantially retained cone photoreceptors with disproportionate cone function loss, such as in the human disease. *NPHP5*- and *NPHP6*-LCA across a wide age spectrum are thus excellent candidates for cone-directed gene augmentation therapy, and the *rd16;Nrl*$^{-/-}$ mouse is an appropriate model for pre-clinical proof-of-concept studies.

INTRODUCTION

Leber congenital amaurosis (LCA) is a genetically heterogeneous retinal blindness detected in infancy (1,2). Whereas one molecular form of LCA (due to mutations in the *RPE65* gene) has been treated safely and successfully using retinal gene therapy (3), there are at least 14 more genetic subtypes. The challenge is now to determine which of these other forms are treatable and how. Among the many scientific and medical hurdles to clear en route to a clinical trial, a very basic one

*To whom correspondence should be addressed at: Scheie Eye Institute, University of Pennsylvania, 51 North 39th Street, Philadelphia, PA 19104, USA. Tel: +1 2156629986; Email: cideciya@mail.med.upenn.edu

demands early attention. When available animal models of a human disease exist, the question should be asked whether there is sufficient similarity between the expressions of the retinal disease in the animals and humans to warrant proof-of-concept experiments in the models.

An LCA disease of strong interest for gene therapy is the most common and a severe molecular form—that associated with *Nephrocystin-6* (*NPHP6*, also known as *CEP290*) mutations (1,4,5). The *NPHP6* gene product is localized primarily to the (connecting) cilium (CC) adjoining the outer segment (OS) to the photoreceptor cell body (6,7), and is thought to be involved in the formation of microtubule-membrane linkers in this region (8). The loss of NPHP6 function may affect cilia biogenesis (9,10), or protein composition of the photoreceptor OS (7,8). NPHP6 interacts with other cilia proteins, including RPGR (7), which, when mutated, causes retinal degeneration (2). As *NPHP6* is expressed in all primary cilia, many mutations cause syndromic diseases involving the central nervous system, kidney and liver, in addition to retinal degeneration (6,11–13). Mutations in *NPHP5* (also known as *IQCB1*) are associated with similar ciliopathies and the encoded nephrocystin also interacts with RPGR (14–16). Mutations in *NPHP5* cause LCA (14,17,18).

What pre-clinical models are available for proof of concept in *NPHP5*- and *NPHP6*-LCA? An alga mutant with a large deletion in the *NPHP6* homologue shows very short cilia; the phenotype can be corrected when supplied with the wild-type (WT) protein (8). The Nphp6-deficient Abyssinian cat (19) is a large animal model with a disease course that is not reminiscent of human *NPHP6*-LCA. The cat has a relatively slow time course of degeneration, substantial retinal physiological responses and rod visual pigment content until late in the disease (20,21). The *rd16* mutant mouse with a hypomorphic *Nphp6* mutation (7), however, has a rapid retinal degeneration that appears more like the severe and early blindness of the human disease.

We addressed whether human *NPHP5* and *NPHP6*-LCA could be moved closer to being treatable diseases by exploring the fate of rod and cone photoreceptors in humans. Humans with little or no vision still showed some rod cells with abnormalities in the rod OS, but rods disappeared early in life; details of the rod ciliopathy were studied in *rd16* mice. The all-cone human fovea was retained in humans at most ages despite the disproportionate vision loss. In order to model the retained foveal cones in patients, we generated mice with all-cone retinas and *Nphp6* dysfunction by crossing *rd16* mice (7) with $Nrl^{-/-}$ mice (22). An extreme dissociation of cone function and structure in the $rd16;Nrl^{-/-}$ retina, like that in the human ciliopathies, was identified, as well as salient features of the cone pathogenesis. We conclude that the next and most expeditious experimental steps leading to a human clinical trial would best be performed on a mammalian model, such as the $rd16;Nrl^{-/-}$ double-mutant mouse, with cone function as the metric of importance.

RESULTS

Rod photoreceptors develop but degenerate rapidly in human LCA with *NPHP5* or *NPHP6* mutations

NPHP5- or *NPHP6*-LCA cause congenital blindness due to photoreceptor malfunction, but details of the disease in the rods, representing ∼94% of human retinal photoreceptors (23), are unknown. Whether rod photoreceptors even develop in the human diseases is unknown—a critical fact for designing realistic therapies for these forms of LCA. Most of the human mutant retinas we studied showed no detectable photoreceptors outside the central region. Surprisingly, in the mid-peripheral retina of two young patients (*NPHP6*-P2, age 8, and *NPHP5*-P16, age 7, Table 1), the outer nuclear layer (ONL), the retinal layer comprised of photoreceptor nuclei, was clearly visible starting at 5–6 mm eccentricity from the fovea (Fig. 1A). A region of major photoreceptor loss, with barely detectable ONL and little or no discernible inner segment (IS) and OS, was present between the retained center and mid-peripheral ONL (Fig. 1A). In *NPHP5*-P16, spatial topography of ONL thickness across a large expanse of the retina showed a wide annular region lacking photoreceptors and encircled by a mid-peripheral region of retained ONL (Fig. 1B). In contrast, *NPHP6*-P3 at age 10 had barely detectable ONL in the mid-peripheral regions (Fig. 1A).

Quantitative signal processing of longitudinal reflectivity profiles (LRPs) in the superior and inferior regions with ONL between eccentricities of 7–9 mm (Fig. 1A, white rectangles) were performed. Unexpectedly, several retinal laminae in P2 and P16 were thicker than normal. These thicker layers included the outer plexiform layer (OPL) where photoreceptors synapse to secondary neurons, and the inner nuclear layer (INL) where bipolar, Müller cell and other nuclei normally reside (Table 2). Also, ONL thickness in both patients was at the upper limit of normal or greater than normal (Table 2). At this retinal eccentricity, rods outnumber cones 28:1 in normal human retinas (23); thus, the dominant cell in the ONL would be rod photoreceptor nuclei. Thickening of layers has been suggested to represent the earliest signs of photoreceptor stress, and a phase that precedes rapid photoreceptor degeneration (24–27).

The structural abnormalities distal to the rod photoreceptor nuclei between the ONL and retinal pigment epithelium (RPE) were studied with quantitative LRP analysis in superior and inferior retinal regions (Fig. 1C). In normal retinas, there are distinct local backscatter peaks associated with the outer limiting membrane (OLM) forming the intercellular adherens junctions between photoreceptors and Müller glia; the junction at the CC between IS and OS; and reflections originating near the apical boundary of the RPE and between RPE and Bruch membrane (Fig. 1C). In P2 and P16, however, these peaks are replaced with a region of similar thickness but with diffusely increased light scatter (S+) likely originating from abnormal rod IS/OS (Fig. 1C).

Rods past: the history of photoreceptors imprinted in the RPE of *NPHP5*- and *NPHP6*-mutant eyes

In retinas devoid of rod photoreceptors, we searched for their ‘tombstones’ within RPE cells which can survive for decades even after the loss of photoreceptors. Lipofuscin, an RPE pigment (28), continuously accumulates with age through phagocytosis of OS tips that contain the photoisomerization product all-*trans* retinal generated during the retinoid cycle of vision (29). In normal eyes, RPE lipofuscin distribution

Table 1. Clinical and molecular characteristics of patients

Patient	Age (years)/gender	Nucleotide change[a]	Protein change	Visual acuity[b]		Refraction[c]		Kinetic visual field extent (V-4e)[d]		ERG	FST[e]
				RE	LE	RE	LE	RE	LE		
NPHP6 (CEP290)											
P1[f]	7/M	c.2991+1655A>G c.2507_2508delAG	Splice defect[g] p.T835fs	NLP	NLP	+7.00	+7.75	ND	ND	ND	N/A
P2	8/M	c.2991+1655A>G c.289G>T	Splice defect[g] p.E97X	NLP	NLP	+7.00	+7.00	ND	ND	ND	N/A
P3	10/F	c.2991+1655A>G c.1550delT	Splice defect[g] p.L517fs	LP	LP	+8.00	+7.25	ND	ND	ND	C; −7.3
P4[f]	11/F	c.2991+1655A>G c.2991+1655A>G	Splice defect[g] Splice defect[g]	HM	HM	+5.25	N/A	ND	ND	ND	R and C; −4.4
P5[f]	14/M	c.2991+1655A>G c.4882C>T	Splice defect[g] p.Q1628X	NLP	NLP	+5.50	+5.50	ND	ND	ND	N/A
P6[f,h]	17/M	c.2991+1655A>G c.5668G>T	Splice defect[g] p.G1890X	20/1200	20/800	+6.50	+4.50	ND	ND	ND	R and C; −4.6
P7[f,h]	19/F	c.2991+1655A>G c.5668G>T	Splice defect[g] p.G1890X	20/63	20/50	+2.75	+3.25	13	15	ND	C; −4.0
P8[i]	19/M	c.2991+1655A>G c.5493delA	Splice defect[g] p.Q1830fs	NLP	NLP	+11.00	+11.00	ND	ND	N/A	N/A
P9[f]	20/F	c.2991+1655A>G c.2991 + 1655A > G	Splice defect[g] Splice defect[g]	20/400	20/50	+7.75	+4.00	8	8	ND	C; −4.2
P10[i]	24/F	c.2991+1655A>G c.5493delA	Splice defect[g] p.Q1830fs	NLP	LP	+8.50	+7.50	ND	ND	ND	N/A
P11[f]	26/M	c.2991+1655A>G c.1260_1264delTAAAG	Splice defect[g] p.T420fs	LP	LP	+4.00	+4.00	2	4	N/A	C; −5.0
P12[j]	27/F	c.3175_3176insA c.7341_7342insA	p.I1059fs p.L2448fs	20/800	20/800	+3.00	+3.00	<1	<1	ND	C; −4.9
P13	33/M	c.2991+1655A>G c. 4723A>T	Splice defect[g] p.K1575X	HM	HM	0.00	0.00	ND	ND	ND	C; −5.2
P14[f]	48/M	c.2991+1655A>G c.2390delA	Splice defect[g] p.K797fs	NLP	NLP	+6.00	+6.00	ND	ND	N/A	N/A
NPHP5 (IQCB1)											
P15[k]	5/M	c.1465C>T c.1516_1517delCA	p.R489X p.H506del2cagCA	LP	LP	+7.50	+7.50	ND	ND	N/A	N/A
P16	7/M	c.1516_1517delCA c.1516_1517delCA	p.H506del2cagCA p.H506del2cagCA	20/400	20/800	+6.00	+6.00	ND	ND	ND	R and C; −3.6
P17[k]	8/M	c.1465C>T c.1516_1517delCA	p.R489X p.H506del2cagCA	LP	LP	+9.00	+9.00	ND	ND	N/A	N/A
P18	13/M	c.1381C>T c.1516_1517delCA	p.R461X p.H506del2cagCA	20/200	20/200	+4.00	+4.00	<1	<1	ND	C; −4.8
P19[l]	23/F	c.333delT c.1381C>T	p.A111del1gcT p.R461X	20/80	20/200	+1.00	+1.00	<1	<1	ND	C; −4.7

RE, right eye; LE, left eye; ND, not detectable; N/A, not available; HM, hand motions; LP, light perception; NLP, no light perception.
[a]Nucleotide positions are based on GenBank sequence NM_025114.3 (*NPHP6/CEP290*), NM_001023571 (*NPHP5/IQCB1*), with the A of the start codon (ATG) designated as +1.
[b]Best corrected visual acuity.
[c]Spherical equivalent.
[d]Expressed as a percentage of normal mean of V-4e target; 2 SD below normal equals 90%.
[e]Loss of full-field sensitivity (FST) compared with normal in $\log_{10}$ units and type of photoreceptor mediation; R, rod, C, cone.
[f]Patients previously published in Cideciyan *et al.*[31]
[g]Creates a new splice site in intron 26 that causes a premature stop at position 998.
[h,i,k]Patients are siblings.
[j]Joubert syndrome.
[l]Senior–Loken syndrome.

revealed by short-wavelength autofluorescence (SW-AF) imaging shows a low signal at the fovea, gradually increasing to a maximum at ∼2–6 mm eccentricity, and then decreasing towards the periphery (Fig. 2A, left). This topography is similar to the spatial density of rod photoreceptors in human retinas (23).

Intraretinal variations of RPE lipofuscin signal in *NPHP5*-P16 (Fig. 2A, right) can be interpreted in terms of its co-localization with photoreceptor topography (Fig. 1B). Centrally, there is an ∼3 mm wide elliptical region of low SW-AF intensity similar to that in normal individuals (Fig. 2A); this region corresponds to the retained central island of

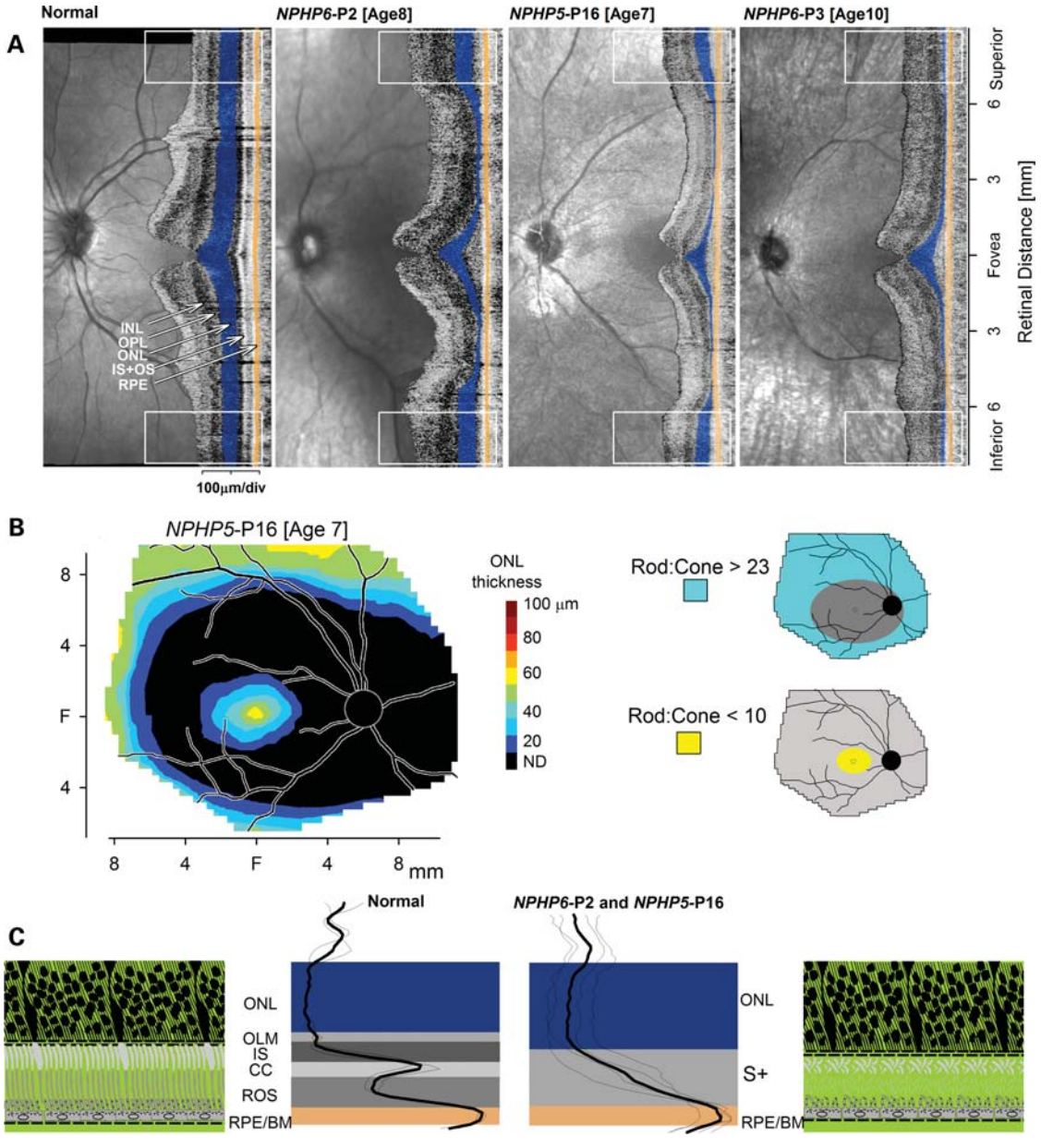

Figure 1. Evidence for rods in *NPHP5 (IQCB1)*- and *NPHP6 (CEP290)*-LCA. (**A**) *En face* images of the fundus of a normal subject (age 15), and three patients: *NPHP6*-P2 (age 8), *NPHP5*-P16 (age 7) and *NPHP6*-P3 (age 10). Overlaid are cross-sectional scans along the vertical meridian through the fovea. Arrows indicate the lamina corresponding to INL, OPL, ONL and RPE. ONL is colorized blue and RPE is colorized orange. Rectangles show superior and inferior regions quantified in (**B**). (B) ONL thickness topography of *NPHP5*-P16 shows the distribution of the detectable photoreceptors to be limited to a central ellipse corresponding to the cone-dominant (Rod:Cone < 10, from ref. 23) region (inset lower right) and more peripherally corresponding to the rod-dominant (Rod:Cone > 23) region (inset upper right). Wide annular region shows no detectable photoreceptors (black). (**C**) The hypothesized mid-peripheral retinal architecture (schematics with green background) corresponding to the LRPs originating distal to the OPL in the normal subject and in P2 and P16. Inferior retinal signals have been stretched by 1.2X in all subjects to compensate for the thinner ONL in this region compared with the superior retina. The wide hyperscattering band (S+) in patients between the ONL and RPE likely corresponds to abnormal photoreceptor segments.

photoreceptors dominated by cones (Fig. 1B). Peripherally, a distinct elliptical hyperautofluorescent boundary ~15 mm wide and ~11 mm high (Fig. 2A) co-localizes with the beginning of retained photoreceptors in an area dominated by rods. Further eccentric to the boundary, SW-AF intensity is lower but still higher than normal. Unexpectedly, between the central and peripheral regions, there is an intervening annulus with a detectable lipofuscin signal (Fig. 2A) but no detectable photoreceptors (Fig. 1B). This region likely contained photoreceptors that have since degenerated (Supplementary Material, Fig. S1; Supplementary Text). The accumulated lipofuscin provides support for previous synthesis of its diretinal bisretinoid precursors within photoreceptors. These precursors, in turn, would have required the generation of all-*trans* retinal from photoisomerization of the retinal chromophore after absorption of light within the mutant photoreceptor OS.

Table 2. Thickness of retinal layers in patients with *NPHP5*- or *NPHP6*-LCA and detectable photoreceptors at 7–9 mm eccentricity

	ONL thickness (μm)	OPL thickness (μm)	INL thickness (μm)
Superior retina			
NPHP6-P2	67	33	46
NPHP5-P16	59	28	34
NPHP6-P3	9	12	37
Normal (mean ± 2SD)	50 ± 15	17 ± 5	22 ± 6
Inferior retina			
NPHP6-P2	53	34	34
NPHP5-P16	59	25	28
NPHP6-P3	12	18	26
Normal (mean ± 2SD)	42 ± 9	20 ± 9	22 ± 6

Three other patients illustrate RPE lipofuscin distribution at different stages of *NPHP5*- and *NPHP6*-LCA disease. *NPHP6*-P10 (age 26) shows RPE lipofuscin topography with a broad annulus of higher signal at eccentricities beyond ~1 mm; reduction of signal near the fovea centralis is expected from the absorption of macular pigment and RPE melanin (Fig. 2B). Quantitatively, lipofuscin autofluorescence intensity along the horizontal meridian is near the upper limits of normal (Fig. 2C); most of the central retina has retained detectable photoreceptors (nuclei and a layer of abnormal IS and OS) even though the patient has no perception of light (Table 1). RPE lipofuscin topography in P10 differs substantially from that in other genetic retinal degenerative conditions associated with severe visual loss (Supplementary Material, Fig. S2; Supplementary Text).

NPHP6-P7 (age 19) and *NPHP5*-P19 (age 23) demonstrate more advanced disease stages having smaller extents of detectable photoreceptors (Fig. 2C). Large regions devoid of photoreceptors surrounding the central elliptical islands have surprisingly high lipofuscin signaling (Fig. 2B). Quantitatively, lipofuscin intensity is mostly within normal limits (Fig. 2C). Along a subset of meridians, both P7 and P19 show a narrow intermittent hyperautofluorescent band near the edge of the central region of retained photoreceptors and the surrounding region of neurodegeneration (Fig. 2B). In P19, a further disease boundary is apparent peripherally where spatially heterogenous RPE atrophy starts with concordant lipofuscin loss (Fig. 2B). Melanin topography in all three patients also shows retained RPE with partial demelanization corresponding to the regions devoid of photoreceptors but retained lipofuscin; this validates the interpretation from lipofuscin topography (Supplementary Text). Of note, the pattern of centrally retained photoreceptor and RPE cells would not be surprising in typical retinitis pigmentosa (RP) in which patients have loss of photoreceptors in adult life after decades of useful vision. Retinal regions in RP, not unexpectedly, also show historical evidence of photoisomerizations underlying the vision (Supplementary Material, Fig. S3). In *NPHP5*- and *NPHP6*-LCA, on the other hand, evidence of lipofuscin is unexpected not only because of the profound visual impairment at the time of imaging but also considering a lack of vision even in the first few months of life.

The results in *NPHP5*- and *NPHP6*-LCA indicate that there is differentiation of rod photoreceptors during early development. The distal segments of photoreceptors, however, either do not elaborate normally or they become structurally unstable after maturation causing early and severe loss of visual function. These abnormal rods do not survive and degenerate rapidly within the first decade of life.

Rd16 mouse rods show normal ciliogenesis followed by abnormal elaboration of OS

To examine further the rod abnormalities in NPHP6 deficiency, we took advantage of the rapid rod photoreceptor degeneration in *rd16* mice, which recapitulates *NPHP6*-LCA and probably *NPHP5*-LCA (7). Early photoreceptor development [postnatal day (p) 2 to p8] proceeds normally in the *rd16* mouse retina. Although at p10 (and p12), all layers of the retina were present and grossly normal with IS and OS lengths comparable with the WT (Fig. 3A and B), OS elongation was clearly stalled at p14 and began to regress (Fig. 3B). Simultaneously, pyknotic photoreceptor nuclei appeared in the ONL which started to thin (Fig. 3A and B, arrows). Only about four layers of nuclei remained at p18 (Fig. 3A) with almost complete loss of IS and OS (Fig. 3B). Only a single row of ONL nuclei remained at p28, and these nuclei belonged exclusively to cones (Fig. 3F).

As photoreceptor OS are considered modified primary cilia (30), we examined the CC, basal body (BB) and related structures at the ultrastructural level (Fig. 3C–E). The BB, derived from the mother centriole, anchors and gives rise to the primary cilium, with two distinct parts—CC and ciliary axoneme that provides the backbone for membranous OS discs. The CC is intact and positioned appropriately in *rd16* compared with the WT retina; however, the axoneme is reduced or absent in *rd16* (Fig. 3C, asterisk), a finding consistent with the failure of OS elongation because of a cilial transport defect in *rd16* photoreceptors. Thus, OS remain rudimentary and fail to extend in the *rd16* retina, even though the process of cilia biogenesis is initiated (Fig. 3D and E).

Retained foveal cone photoreceptor nuclei with abnormal IS and OS in *NPHP5*- and *NPHP6*-mutant human retinas

High-resolution imaging at the cone-rich foveal region of human retinas confirmed and extended the puzzling finding of profound blindness in patients with *NPHP6*-LCA despite retained cone photoreceptor nuclei (31). We therefore defined the regions with healthy RPE cells that could support photoreceptors (32) by mapping the melanin pigment they contain (28) using *in vivo en face* near-infrared autofluorescence (NIR-AF) imaging (33). In a normal control subject, thicker foveal RPE cells (34) have the highest melanin optical density and NIR-AF shows the highest intensity at the foveal region with a gradual decline to ~1 mm eccentricity surrounded by homogenous signal; retinal blood vessels and the optic nerve head show low signal (Fig. 4A, left panel). *NPHP6*-LCA patients with profound blindness (Table 1) show melanized and structurally sound RPE within central elliptical regions, which are abruptly delineated and surrounded by abnormally reduced melanin signal as in *NPHP6*-P3 at age 10 (Fig. 4A). We then studied

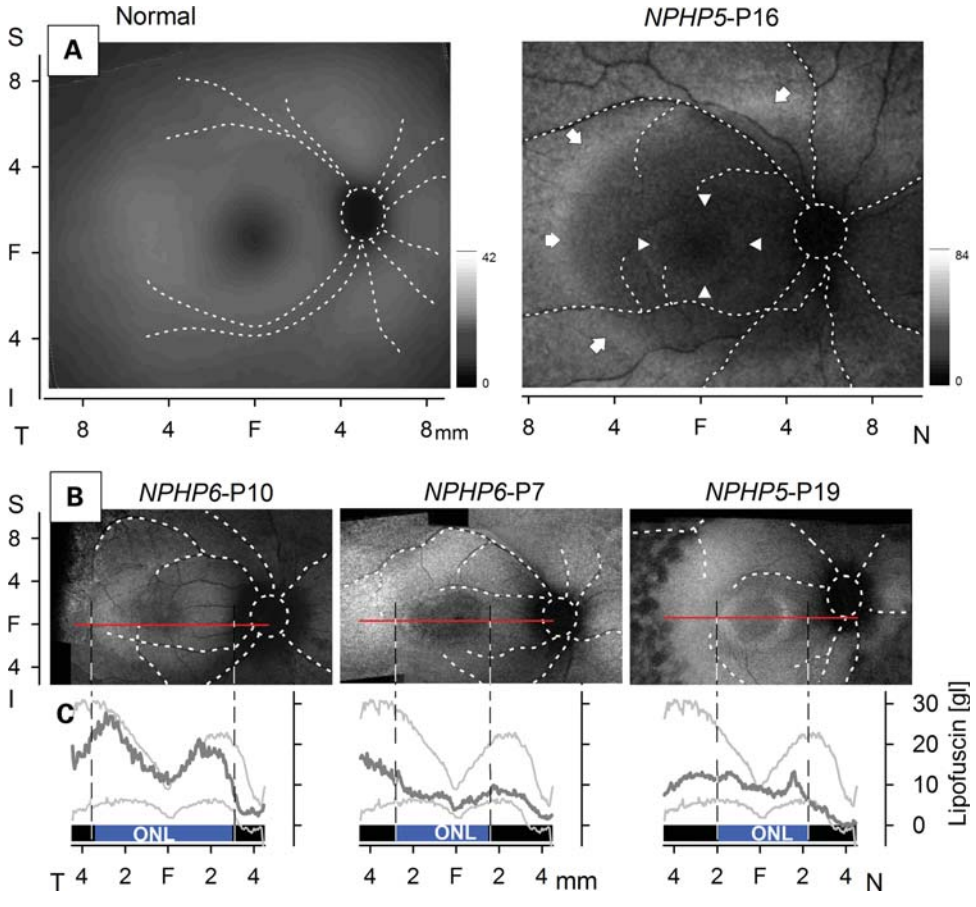

Figure 2. RPE lipofuscin accumulation providing historical evidence for rods in *NPHP5 (IQCB1)*- and *NPHP6 (CEP290)*-LCA. (**A**) Mean RPE lipofuscin topography in normal subjects ($n = 5$) compared with that of *NPHP5*-P16 (age 7). There are concentric elliptical regions consisting of a central darker region (triangles), an intermediate region and a bright region (arrowheads). Note the 2× difference in grayscales used. (**B**) RPE lipofuscin topography in three patients with *NPHP5*- or *NPHP6*-LCA shows nearly normal distribution in P10 and annuli of relative hyperfluorescence surrounding a central ellipse in P7 and P19. Further towards the periphery, P19 shows autofluorescence results typical of RPE atrophy. Red lines show the location and extent of the region quantified in (C). (**C**) Semi-quantitative lipofuscin intensity (gray level, gl) across the horizontal meridian crossing the fovea in three patients (thick dark gray traces) compared with normal limits (±2 SD, pair of thin light gray traces). Bars demarcate regions of detectable (blue) and undetectable (black) ONL.

cross-sectional retinal scans to understand the architecture of retinal layers. In the normal eye, the ONL (highlighted blue, Fig. 4B) contains cone photoreceptor nuclei at the fovea and both rod and cone nuclei surrounding the fovea; the ratio of cone to rod densities decreases with eccentricity (23). *NPHP6*-P3 shows normal ONL thickness at the fovea (Fig. 4B), but gradual thinning of ONL with increasing eccentricity, as would be expected from a retina that had lost rod nuclei but retained cone nuclei. Most *NPHP6*-LCA patients showed a detectable ONL at the fovea and gradual thinning with eccentricity (31). The retinal phenotype of *NPHP5*-LCA with *en face* NIR-AF and cross-sectional imaging was similar to that in patients with *NPHP6* mutations (14–18). *NPHP5*-17 (age 8), for example, had profound blindness (Table 1), retained melanized RPE within a central elliptical region surrounded by abnormally reduced melanin (Fig. 4A) and partially retained ONL thickness at the fovea that gradually thinned with eccentricity (Fig. 4B). All *NPHP5*-LCA patients showed a similar pattern.

To better understand the relationship between the severe visual loss despite retained cone photoreceptor nuclei, we performed quantitative signal processing (25). In normal foveas, local backscatter characteristics (peaks and troughs) occur distal to the ONL in association with the OLM, CC and reflections originating near the apical and basal boundaries of the RPE (Fig. 4C). Foveal LRPs from *NPHP5*- and *NPHP6*-LCA patients (P3, P15, P17 and P18) show the replacement of the distinct OLM and CC signals with a wide band of high backscatter (S+) and a narrower band of low backscatter (S−) between the ONL and the RPE, likely representing remnants of photoreceptor IS and/or OS (Fig. 4C). These results suggest that structural abnormalities occurring distal to the cone photoreceptor nuclei between the ONL and the RPE may contribute to the profound blindness experienced by the patients despite retained photoreceptor nuclei (Fig. 4C).

A mouse model relevant to *NPHP5*- and *NPHP6*-LCA human clinical trials

Our finding of early rod loss but decades-long retention of central cone nuclei in *NPHP5*- and *NPHP6*-LCA strongly argues the need for an animal model with a similar phenotype for the design and testing of human treatments. *Rd16* mice show only a single row of cone nuclei remaining after rod

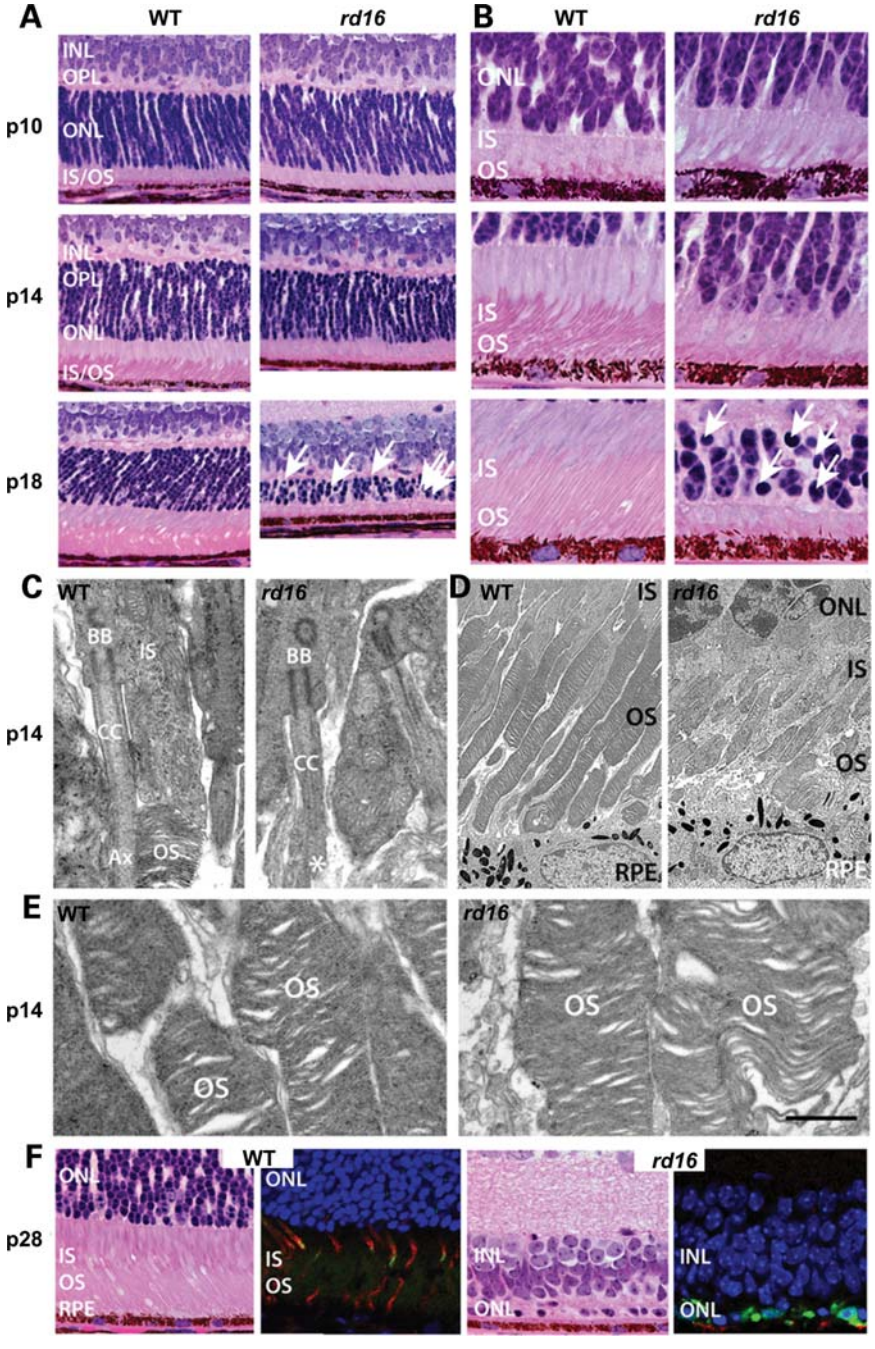

Figure 3. Evidence of OS formation, followed by rapid rod degeneration in *rd16* mutant mice. (**A** and **B**) Histological sections of the superior central retina at the level of the optic nerve head from p10, p14 and p18. H&E (A) or higher magnification PAS (B) stained images show the time course of rapid photoreceptor degeneration in *rd16* mice. Arrows, apoptotic profiles. (**C**) Transmission EM images illustrating the presence of BB and CC at the IS/OS junction at p14. (**D** and **E**) Stacks of OS are formed in *rd16* retinas but do not organize into the extended vertical arrays typically seen in WT mice. Notably, this initial structural normalcy ends abruptly when the OS should progressively elongate, suggesting that the Nphp6 mutation in *rd16* mice abrogates axoneme extension, and that the failure to complete OS morphogenesis leads to rapid cell death. (**F**) In p28 *rd16* retina, rod photoreceptors have completely degenerated and only a single layer of cone nuclei remains in the ONL (red, cone arrestin, green, PNA).

degeneration (Fig. 3F) and at 6 weeks of age show minimal S- and M-cone-mediated electroretinography (ERG) responses that are near recording noise level and, at best, are 0.9–1.3 log units smaller than WT responses (Fig. 4D and E). To generate an improved mouse model with an enriched cone population for testing treatment efficacy, we generated *rd16;Nrl*$^{-/-}$ double-mutant mice by breeding *rd16* mice with the cone-only *Nrl*$^{-/-}$ mice (22,35). *Rd16;Nrl*$^{-/-}$ double-mutant mice (ages 2.5–4 months) showed sizeable S- and M-cone-driven ERG signals, although the amplitudes were reduced on average by 1 log unit compared with *Nrl*$^{-/-}$ mice (Fig. 4D and E).

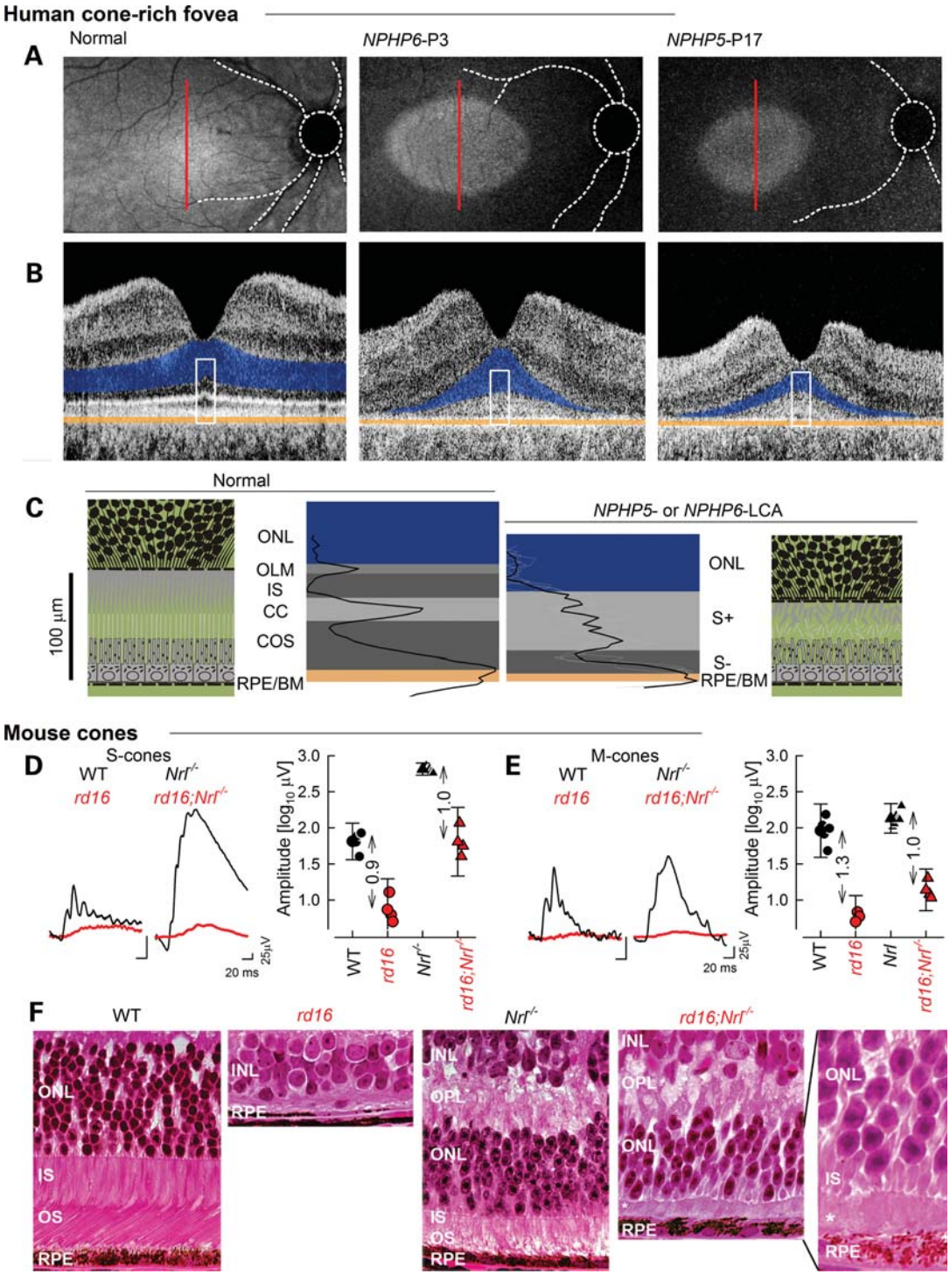

Figure 4. Loss of cone function despite retained cone photoreceptors in *NPHP5 (IQCB1)*- and *NPHP6 (CEP290)*-mutant human and *Nphp6 (Cep290)*-mutant mouse retinas. (**A**) Cone-rich fovea and surrounding central retina in a normal subject compared with patients with *NPHP5*- or *NPHP6*-LCA. RPE melanization is retained in an elliptical region of the central retina as determined with *en face* NIR-AF imaging. Retinal blood vessels and the optic nerve head correspond to low signal and are outlined (white dashed lines). Red lines show the location and extent of the vertical scans shown in (B). (**B**) Cross-sectional scans along the vertical meridian crossing the fovea. ONL is highlighted (blue). White rectangles delineate the foveal region shown in (C). (**C**) Hypothesized foveal retinal architecture (schematics with green background) corresponding to the LRPs originating distal to the ONL in the normal subject and the average from four patients with *NPHP5*- and *NPHP6*-LCA (P3, P15, P17 and P18). Lamina corresponding to OLM, IS, CC, COS and RPE in the normal eyes are shown. There are wide hyperscattering (S+) and thinner hyposcattering (S−) bands in patients. (**D** and **E**) S- and M-cone photoreceptor-driven ERGs are substantially smaller in *rd16* or *rd16;Nrl*$^{-/-}$ (red traces) than in the WT or *Nrl*$^{-/-}$ (black traces). Quantitative analysis (right panels in D and E) shows 0.9–1.3 $\log_{10}$ reduction in ERG amplitudes associated with Nphp6 deficiency when compared with WT and *Nrl*$^{-/-}$ controls. (**F**) Retinal sections at 3–4 months demonstrate complete photoreceptor loss in *rd16* mice compared with the rod-dominant WT mouse retina. In contrast, *rd16;Nrl*$^{-/-}$ retinas retain significant numbers of cone nuclei almost to the same extent as *Nrl*$^{-/-}$ control retinas at this age. The segment layers, indicated by an asterisk, are not well-defined; however, some IS are found within the ONL.

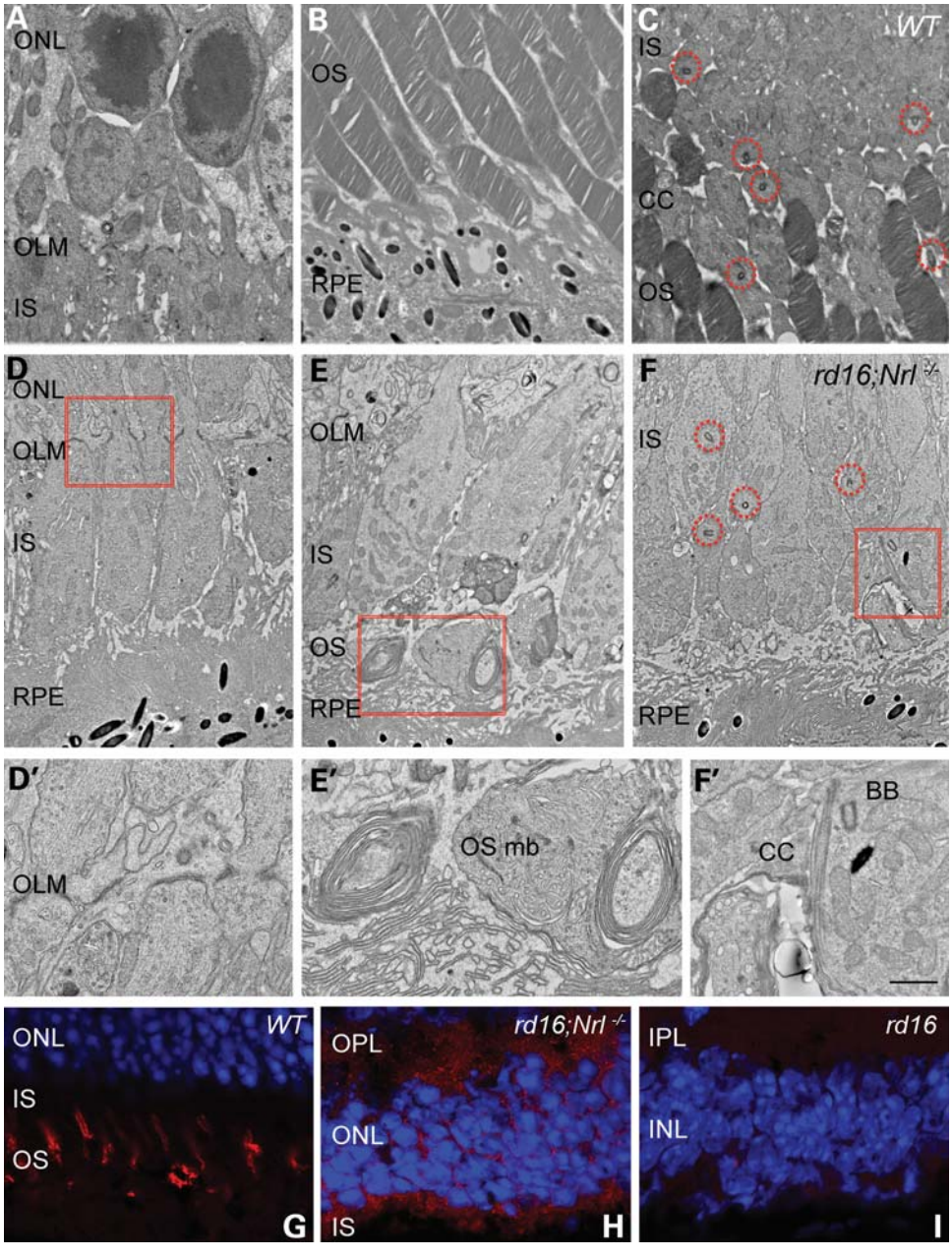

Figure 5. Ultrastructure and S-opsin immunoreactivity of *rd16;Nrl*$^{-/-}$ cone photoreceptors. (**A**–**C**) Structure of outer retinal features in the WT mouse. (**D** and **D′**) *Rd16;Nrl*$^{-/-}$ cones showing that the OLM and IS are present. (**E** and **E′**) The OS membrane (OS mb), however, is barely detectable. (**F** and **F′**) Frequent BB and infrequent CC form, suggesting that abnormal OS formation is not due to lack of proximal structures. (**G**–**I**) Confocal images of S-opsin immunoreactivity in the WT at 1 month, and in *rd16;Nrl*$^{-/-}$ and *rd16* retinas at 3–4 months. In the WT retina, cone OS are distinctly labeled. In the *rd16;Nrl*$^{-/-}$ retina, opsin immunoreactivity localizes to the cell body, whereas it is absent by this age in the *rd16* retina as all photoreceptors have degenerated. Scale bar, 2 μm.

We detected significant survival of cone photoreceptors in the *rd16;Nrl*$^{-/-}$ retina; histology of the eyes shows four to five rows of ONL nuclei (Fig. 4F) at 3–4 months of age (equivalent to a young adult human) when all photoreceptors have degenerated in the *rd16* retina. Electron microscopy of *rd16;Nrl*$^{-/-}$ photoreceptors shows IS with a distinct OLM (Fig. 5A, D, D′), and rare OS with scant OS-like membranes (Fig. 5B, E, E′). BB and occasional CC, however, were observed (Fig. 5C, F, F′). In 3-month-old *rd16;Nrl*$^{-/-}$ photoreceptors, S-opsin localizes to the cell body and the OPL region instead of the OS as in the WT retina. Notably, no S-opsin is detected in the *rd16* retina at this age, consistent with the absence of photoreceptors (Fig. 5G–I).

DISCUSSION

Rod photoreceptor cells develop but die rapidly in human *NPHP5*- and *NPHP6*-mutant retinas

Here we report finding rod structure in human *NPHP5*- and *NPHP6*-mutant retinas. The ONL could be retained in a region of high rod density in some young patients, indicating

that rod photoreceptors did develop. These data demonstrate that rod cell loss is the ultimate fate due to a rapid yet progressive degeneration. An alternative hypothesis of rod agenesis due to a possible centrosomal role of NPHP6 (7,11) is not supported. Lipofuscin detected in the RPE in the absence of photoreceptors provides further evidence that rods had produced OS and photoisomerization occurred at an early disease stage. The hyper-reflective layer defined by *in vivo* microscopy between the ONL and the RPE suggests remnants of IS and OS material. The *rd16* mouse histopathology was consistent with the human data in showing disorganized and truncated rod OS in the second postnatal week. Rapid loss of rods at later ages may be due to the strong dependence of rod cell survival on normal OS development (36).

Sequelae of the early rod cell death in *NPHP5* and *NPHP6* disease and in the *rd16* mouse

Abnormal rod photoreceptor OS are detected before rod cell death in both human *NPHP5*- or *NPHP6*-LCA and mouse *Nphp6*-mutant (*rd16*) retinas. *rd16* rod cells have mislocalization and accumulation of opsin, a frequent finding in animal models of retinal degeneration as well as human retinopathies with or without ciliopathy as a suspected cause (2,37–39). The result in *rd16*, however, suggests a ciliary transport abnormality due to altered Nphp6 function. Recently, knockout mice for the *Ahi1* gene, which also encodes a cilium-localized protein, were shown to have no rod OS formation and a rapid retinal degeneration with abnormal distribution of opsin throughout photoreceptors (40). Genetically engineered reduction of the opsin dosage in the $Ahi1^{-/-}$ mice led to the same OS formation defect but delayed retinal degeneration, suggesting that the secondary opsin accumulation contributed to cell death. Hence, disrupted intraflagellar transport and defective localization of OS components, key to the normal function and structure of photoreceptors, may be triggers for apoptotic rod cell death (41) in the *NPHP5*- and *NPHP6*-mutant retinas.

Secondary to the relatively rapid rod cell death, we noted abnormal thickening of retinal layers in the human retinas with *NPHP5* or *NPHP6* mutations. Neuronal damage in the mature central nervous system elicits complex remodeling responses of neurons and glia, as documented in animal retinae with genetic or traumatic disease (42,43) and in post-mortem human donor retinas affected with retinal degeneration (38). Using *in vivo* microscopy in several human retinal diseases, we found unexpected and dramatic retinal thickening, primarily of the INL, that we attribute to Müller glial cell activation following photoreceptor stress (24,25,27,31). This retinal thickening appears to be a marker of an early disease stage of remodeling. A signaling pathway involving injured photoreceptors and Müller cells has been elucidated (44). Our studies indicate that photoreceptor stress or loss in *NPHP5*- or *NPHP6*-mutant retinas leads to Müller cell activation, hypertrophy or possibly proliferation, and this is detectable as retinal thickening by *in vivo* cross-sectional imaging. Intracellular edema of neuronal or glial cells may also contribute to retinal thickening, as suggested by studies of neurotrophic factors in retinal degenerations (45).

We previously reported that INL thickening in *NPHP6*-LCA has a correlate in *rd16* retina (31). Increased ONL thickening in retinal regions with high rod:cone ratios, however, has not been observed in the human retina until the present study. ONL thickening was found in the canine retina with *RPGR* mutations treated with ciliary neurotrophic factor and an abnormal increase in rods was documented (45). We speculate that the possible thickening of ONL in the human retinas with NPHP5 or NPHP6 defects results from endogenous release of neurotrophic factors after photoreceptor stress, dysfunction or death. Alternatively or additionally, co-localized thickening of ONL, OPL and INL could be secondary to Muller glial cell activation, hypertrophy or possibly proliferation (see above). Observed hyperautofluorescence, which could signal oxidation of the RPE lipofuscin that has accumulated (29), is also consistent with the existence of outer retinal stress in these regions.

Extended survival of dysfunctional photoreceptors in cone-only retinal environment

Photoreceptors detected in most of the *NPHP5*- and *NPHP6*-mutant human retinas were at and near the cone-rich human fovea. For many human retinal degenerations in the RP spectrum and their animal models, it is not uncommon for relatively rapid rod photoreceptor degeneration to be followed by a much slower cone loss (38). What is unusual in the *NPHP5*- and *NPHP6*-associated ciliopathies is the profound dysfunction of the cone photoreceptors, the nuclei of which continue to be structurally detectable for extended periods. We must point out that not all molecular defects at the cone cilium lead to this unusual phenotype (46). However, to pinpoint the abnormality leading to this unusual phenotype will not be trivial considering more than 600 proteins comprise the cilium, and there is evidence of extensive epistatic interactions among many ciliary proteins (41,47–49).

The *rd16* mouse provides evidence of detectable cone photoreceptors at least for a period after rods had degenerated. However, the mouse retina with a 30:1 rod:cone ratio could not provide a satisfactory comparison to a primate cone-only fovea (50). Some of the cone cell losses observed in both the *rd16* retinas and extra-central human retinas may be due to non-autonomous processes (51,52). This hypothesis suggests that the degeneration of the majority photoreceptor, the rods, has a deleterious effect on the survival of the minority cone population. When the cone-rich double-mutant *rd16;*$Nrl^{-/-}$ mouse was studied, it was clearer that cone cell loss resulting from the Nphp6-defect was slow even though cone dysfunction was quite profound. Similar approaches taking advantage of an all-cone retina of the $Nrl^{-/-}$ mice have been previously used to decipher the primary and secondary disease effects on cone function and survival (36,53–55).

Clinical implications of the human and murine results

We propose that the present series of human and animal experiments serve as a model for how research can be moved more expeditiously toward human clinical trials of retinal degenerative diseases. Our strategy was to define the detailed disease

expression in molecularly clarified humans with blindness and, in parallel, query greater details of mechanism from relevant animal models. Crossing back and forth between human and animal diseases led to a consensus about the most appropriate target retinal cell and mutant animal to begin proof-of-concept studies. Human retinal degenerative diseases have in the past been thought of as clinically- and now molecularly-diagnosed 'black boxes'. It was previously assumed that the only choice was to discover an agent that works in genetically-similar animals and eventually hand it over to clinicians to administer to the blind patients. The very different strategy we have taken in patients with *NPHP5*- or *NPHP6*-LCA has been made possible by sophistication of non-invasive high resolution imaging in human retinal disease (reviewed in 56).

If a gene replacement treatment strategy for *NPHP5*- or *NPHP6*-LCA was being planned, for example, we can now state that to target rods, therapy would have to be administered within the first few years of life. In contrast, targeting the cones of the foveal-macular region could be of value across a wide spectrum of disease stages and ages (spanning at least the first four decades of life). The safety outcome for any future clinical trial should include *in vivo* imaging using optical coherence tomography (OCT) scans of the retina, in addition to more routine clinical ocular and systemic examinations. The low level of visual acuity would not be a reliable safety parameter for most of the members of these LCA subgroups. An efficacy outcome for a therapy that targeted rods would have to quantify a change in peripheral rod-mediated visual function or the rate of peripheral retinal degeneration—exceedingly difficult measurements to make in very young and severely visually impaired patients. An efficacy outcome for cone-targeted therapy, on the other hand, could include cone function, preferably measured under observation of the fundus, and in the treated region of the central retina in older subjects who would be the candidates for early phase trials. In addition, traditional measures of visual acuity would be available. Increased cone sensitivity or improved visual acuity would signal that cone photoreceptor function is restored; a subfoveal change to more normal IS/OS laminar architecture would be an objective efficacy outcome.

And which animal model would be most valuable for proof-of-concept experiments? For rod-directed therapies, the *rd16* mutant mouse with the rapid rod degeneration and the Nphp6-deficient Abyssinian cat with the slow disease course could be used for proof-of-concept experiments. Limitations for the *rd16* mice would include the urgency for gene delivery to very young mice and use of certain vector pseudo-types that show faster transgene expression. Limitations for the mutant cats would include extended experimental durations awaiting the efficacy of gene therapy to modify the slow natural progression of retinal degeneration over years. For cone-directed therapies, the ideal model should show a dissociation of cone structure and function and a substantial dynamic range of ERG cone function. The all-cone retina of the *rd16;Nrl*$^{-/-}$ double-mutant mice, with measurable cone cell numbers but severely dysfunctional cones, would fulfill the criterion for a model worth considering for proof-of-concept studies attempting to develop treatment for most ages of patients with *NPHP5*- or *NPHP6*-LCA. The difference of hundreds of microvolts between *Nrl*$^{-/-}$ S- or M-cones and the *rd16*:*Nrl*$^{-/-}$ double-mutant cones would provide a useful dynamic range for testing efficacy of the therapy over the short term.

MATERIALS AND METHODS

Human subjects, retinal cross-sectional, RPE lipofuscin and melanin imaging

Patients with LCA and disease-causing mutations in *NPHP6* ($n = 14$) or in *NPHP5* ($n = 5$) were included (Table 1). Informed consent was obtained. Procedures followed the Declaration of Helsinki guidelines and were approved by the institutional review board. Fourier-domain OCT was used (RTVue-100; Optovue Inc., Fremont, CA, USA) with published recording and analysis techniques to perform retinal cross-sectional imaging (24,25,31,57). RPE lipofuscin and melanin imaging was performed as previously described (24,31,33,58). Details are provided (Supplementary Material).

Animals, histology, immunohistochemistry, electron microscopy and ERG

Mice were kept in standard conditions; all procedures conformed to NIH Animal Care and Use Committee approved protocols. ERGs were performed using a computer-based system in mice after dark-adaptation (>6 h) and anesthesia (ketamine, 65 mg/kg, xylazine, 5 mg/kg, i.p.) as described (59–61). Microscopy was performed as previously described (6,7,13,31,61). Details are provided (Supplementary Material).

SUPPLEMENTARY MATERIAL

Supplementary Material is available at *HMG* online.

ACKNOWLEDGEMENTS

We acknowledge Jun Zhang and Kunio Nagashima for expert assistance with electron microscopy.

Conflict of Interest statement. None declared.

FUNDING

Supported in part by Grousbeck Foundation, intramural funds from the National Eye Institute, Macula Vision Research Foundation, Foundation Fighting Blindness, and Hope for Vision. A.V.C. is a RPB Senior Scientific Investigator.

REFERENCES

1. den Hollander, A.I., Roepman, R., Koenekoop, R.K. and Cremers, F.P. (2008) Leber congenital amaurosis: genes, proteins and disease mechanisms. *Prog. Retin. Eye Res.*, **27**, 391–419.
2. Wright, A.F., Chakarova, C.F., Abd El-Aziz, M.M. and Bhattacharya, S.S. (2010) Photoreceptor degeneration: genetic and mechanistic dissection of a complex trait. *Nat. Rev. Genet.*, **11**, 273–284.
3. Cideciyan, A.V. (2010) Leber congenital amaurosis due to RPE65 mutations and its treatment with gene therapy. *Prog. Retin. Eye Res.*, **29**, 398–427.

4. den Hollander, A.I., Koenekoop, R.K., Yzer, S., Lopez, I., Arends, M.L., Voesenek, K.E., Zonneveld, M.N., Strom, T.M., Meitinger, T., Brunner, H.G. *et al.* (2006) Mutations in the CEP290 (NPHP6) gene are a frequent cause of Leber congenital amaurosis. *Am. J. Hum. Genet.*, **79**, 556–561.
5. Perrault, I., Delphin, N., Hanein, S., Gerber, S., Dufier, J.L., Roche, O., Defoort-Dhellemmes, S., Dollfus, H., Fazzi, E., Munnich, A. *et al.* (2007) Spectrum of NPHP6/CEP290 mutations in Leber congenital amaurosis and delineation of the associated phenotype. *Hum. Mutat.*, **28**, 416.
6. Sayer, J.A., Otto, E.A., O'Toole, J.F., Nurnberg, G., Kennedy, M.A., Becker, C., Hennies, H.C., Helou, J., Attanasio, M., Fausett, B.V. *et al.* (2006) The centrosomal protein nephrocystin-6 is mutated in Joubert syndrome and activates transcription factor ATF4. *Nat. Genet.*, **38**, 674–681.
7. Chang, B., Khanna, H., Hawes, N., Jimeno, D., He, S., Lillo, C., Parapuram, S.K., Cheng, H., Scott, A., Hurd, R.E. *et al.* (2006) In-frame deletion in a novel centrosomal/ciliary protein CEP290/NPHP6 perturbs its interaction with RPGR and results in early-onset retinal degeneration in the rd16 mouse. *Hum. Mol. Genet.*, **15**, 1847–1857.
8. Craige, B., Tsao, C.C., Diener, D.R., Hou, Y., Lechtreck, K.F., Rosenbaum, J.L. and Witman, G.B. (2010) CEP290 tethers flagellar transition zone microtubules to the membrane and regulates flagellar protein content. *J. Cell Biol.*, **190**, 927–940.
9. Tsang, W.Y., Bossard, C., Khanna, H., Peränen, J., Swaroop, A., Malhotra, V. and Dynlacht, B.D. (2008) CP110 suppresses primary cilia formation through its interaction with CEP290, a protein deficient in human ciliary disease. *Dev. Cell*, **15**, 187–197.
10. Kim, J., Krishnaswami, S.R. and Gleeson, J.G. (2008) CEP290 interacts with the centriolar satellite component PCM-1 and is required for Rab8 localization to the primary cilium. *Hum. Mol. Genet.*, **17**, 3796–3805.
11. Valente, E.M., Silhavy, J.L., Brancati, F., Barrano, G., Krishnaswami, S.R., Castori, M., Lancaster, M.A., Boltshauser, E., Boccone, L., Al-Gazali, L. *et al.* (2006) Mutations in CEP290, which encodes a centrosomal protein, cause pleiotropic forms of Joubert syndrome. *Nat. Genet.*, **38**, 623–625.
12. Brancati, F., Barrano, G., Silhavy, J.L., Marsh, S.E., Travaglini, L., Bielas, S.L., Amorini, M., Zablocka, D., Kayserili, H., Al-Gazali, L. *et al.* (2007) CEP290 mutations are frequently identified in the oculo-renal form of Joubert syndrome-related disorders. *Am. J. Hum. Genet.*, **81**, 104–113.
13. McEwen, D.P., Koenekoop, R.K., Khanna, H., Jenkins, P.M., Lopez, I., Swaroop, A. and Martens, J.R. (2007) Hypomorphic CEP290/NPHP6 mutations result in anosmia caused by the selective loss of G proteins in cilia of olfactory sensory neurons. *Proc. Natl Acad. Sci. USA*, **104**, 15917–15922.
14. Otto, E.A., Loeys, B., Khanna, H., Hellemans, J., Sudbrak, R., Fan, S., Muerb, U., O'Toole, J.F., Helou, J., Attanasio, M. *et al.* (2005) Nephrocystin-5, a ciliary IQ domain protein, is mutated in Senior-Loken syndrome and interacts with RPGR and calmodulin. *Nat. Genet.*, **37**, 282–288.
15. Schäfer, T., Pütz, M., Lienkamp, S., Ganner, A., Bergbreiter, A., Ramachandran, H., Gieloff, V., Gerner, M., Mattonet, C., Czarnecki, P.G. *et al.* (2008) Genetic and physical interaction between the NPHP5 and NPHP6 gene products. *Hum. Mol. Genet.*, **17**, 3655–3662.
16. Murga-Zamalloa, C.A., Swaroop, A. and Khanna, H. (2009) RPGR-containing protein complexes in syndromic and non-syndromic retinal degeneration due to ciliary dysfunction. *J. Genet.*, **88**, 399–407.
17. Estrada-Cuzcano, A., Koenekoop, R.K., Coppieters, F., Kohl, S., Lopez, I., Collin, R.W., De Baere, E., Roeleveld, D., Marek, J., Bernd, A. *et al.* (2010) IQCB1 mutations in patients with Leber congenital amaurosis. *Invest. Ophthalmol. Vis. Sci.*, Epub ahead of print.
18. Stone, E.M., Cideciyan, A.V., Aleman, T.S., Scheetz, T.E., Sumaroka, A., Ehlinger, M.A., Schwartz, S.B., Fishman, G.A., Traboulsi, E.I., Lam, B.L. *et al.* (2011) Variations in NPHP5 in patients with nonsyndromic Leber congenital amaurosis (LCA) and Senior-Loken syndrome. *Arch. Ophthalmol.*, **129**, 81–87.
19. Menotti-Raymond, M., David, V.A., Schäffer, A.A., Stephens, R., Wells, D., Kumar-Singh, R., O'Brien, S.J. and Narfström, K. (2007) Mutation in CEP290 discovered for cat model of human retinal degeneration. *J. Hered.*, **98**, 211–220.
20. Jacobson, S.G., Kemp, C.M., Narfstrom, K. and Nilsson, S.E. (1989) Rhodopsin levels and rod-mediated function in Abyssinian cats with hereditary retinal degeneration. *Exp. Eye Res.*, **49**, 843–852.
21. Kang Derwent, J.J., Padnick-Silver, L., McRipley, M., Giuliano, E., Linsenmeier, R.A. and Narfström, K. (2006) The electroretinogram components in Abyssinian cats with hereditary retinal degeneration. *Invest. Ophthalmol. Vis. Sci.*, **47**, 3673–3682.
22. Mears, A.J., Kondo, M., Swain, P.K., Takada, Y., Bush, R.A., Saunders, T.L., Sieving, P.A. and Swaroop, A. (2001) Nrl is required for rod photoreceptor development. *Nat. Genet.*, **29**, 447–452.
23. Curcio, C.A., Sloan, K.R., Kalina, R.E. and Hendrickson, A.E. (1990) Human photoreceptor topography. *J. Comp. Neurol.*, **292**, 497–523.
24. Aleman, T.S., Cideciyan, A.V., Sumaroka, A., Windsor, E.A., Herrera, W., White, D.A., Kaushal, S., Naidu, A., Roman, A.J., Schwartz, S.B. *et al.* (2008) Retinal laminar architecture in human retinitis pigmentosa caused by rhodopsin gene mutations. *Invest. Ophthalmol. Vis. Sci.*, **49**, 1580–1590.
25. Jacobson, S.G., Aleman, T.S., Sumaroka, A., Cideciyan, A.V., Roman, A.J., Windsor, E.A., Schwartz, S.B., Rehm, H.L. and Kimberling, W.J. (2009) Disease boundaries in the retina of patients with Usher syndrome caused by MYO7A gene mutations. *Invest. Ophthalmol. Vis. Sci.*, **50**, 1886–1894.
26. Beltran, W.A., Acland, G.M. and Aguirre, G.D. (2009) Age-dependent disease expression determines remodeling of the retinal mosaic in carriers of RPGR exon ORF15 mutations. *Invest. Ophthalmol. Vis. Sci.*, **50**, 3985–3995.
27. Jacobson, S.G. and Cideciyan, A.V. (2010) Treatment possibilities for retinitis pigmentosa. *N. Engl. J. Med.*, **363**, 1669–1671.
28. Feeney, L. (1978) Lipofuscin and melanin of human retinal pigment epithelium. Fluorescence, enzyme cytochemical, and ultrastructural studies. *Invest. Ophthalmol. Vis. Sci.*, **17**, 583–600.
29. Sparrow, J.R., Yoon, K.D., Wu, Y. and Yamamoto, K. (2010) Interpretations of fundus autofluorescence from studies of the bisretinoids of retina. *Invest. Ophthalmol. Vis. Sci.*, **51**, 4351–4357.
30. Insinna, C. and Besharse, J.C. (2008) Intraflagellar transport and the sensory outer segment of vertebrate photoreceptors. *Dev. Dyn.*, **237**, 1982–1992.
31. Cideciyan, A.V., Aleman, T.S., Jacobson, S.G., Khanna, H., Sumaroka, A., Aguirre, G.K., Schwartz, S.B., Windsor, E.A., He, S., Chang, B. *et al.* (2007) Centrosomal-ciliary gene CEP290/NPHP6 mutations result in blindness with unexpected sparing of photoreceptors and visual brain: implications for therapy of Leber congenital amaurosis. *Hum. Mutat.*, **28**, 1074–1083.
32. Bok, D. (1993) The retinal pigment epithelium: a versatile partner in vision. *J. Cell Sci. Suppl.*, **17**, 189–195.
33. Gibbs, D., Cideciyan, A.V., Jacobson, S.G. and Williams, D.S. (2009) Retinal pigment epithelium defects in humans and mice with mutations in MYO7A: imaging melanosome-specific autofluorescence. *Invest. Ophthalmol. Vis. Sci.*, **50**, 4386–4393.
34. Friedman, E. and Ts'o, M.O. (1968) The retinal pigment epithelium. II. Histologic changes associated with age. *Arch. Ophthalmol.*, **79**, 315–320.
35. Daniele, L.L., Lillo, C., Lyubarsky, A.L., Nikonov, S.S., Philp, N., Mears, A.J., Swaroop, A., Williams, D.S. and Pugh, E.N. Jr. (2005) Cone-like morphological, molecular, and electrophysiological features of the photoreceptors of the Nrl knockout mouse. *Invest. Ophthalmol. Vis. Sci.*, **46**, 2156–2167.
36. Farjo, R., Skaggs, J., Nagel, B., Quiambao, A., Nash, Z., Fliesler, S. and Naash, M. (2006) Retention of function without normal disc morphogenesis occurs in cone but not rod photoreceptors. *J. Cell Biol.*, **173**, 59–68.
37. Olsson, J.E., Gordon, J.W., Pawlyk, B.S., Roof, D., Hayes, A., Molday, R.S., Mukai, S., Cowley, G.S., Berson, E.L. and Dryja, T.P. (1992) Transgenic mice with a rhodopsin mutation (Pro23His): a mouse model of autosomal dominant retinitis pigmentosa. *Neuron*, **9**, 815–830.
38. Milam, A.H., Li, Z.Y. and Fariss, R.N. (1998) Histopathology of the human retina in retinitis pigmentosa. *Prog. Retin. Eye Res.*, **17**, 175–205.
39. Lee, E.S. and Flannery, J.G. (2007) Transport of truncated rhodopsin and its effects on rod function and degeneration. *Invest. Ophthalmol. Vis. Sci.*, **48**, 2868–2876.
40. Louie, C.M., Caridi, G., Lopes, V.S., Brancati, F., Kispert, A., Lancaster, M.A., Schlossman, A.M., Otto, E.A., Leitges, M., Gröne, H.J. *et al.* (2010) AHI1 is required for photoreceptor outer segment development and is a modifier for retinal degeneration in nephronophthisis. *Nat. Genet.*, **42**, 175–180.
41. Lancaster, M.A. and Gleeson, J.G. (2009) The primary cilium as a cellular signaling center: lessons from disease. *Curr. Opin. Genet. Dev.*, **19**, 220–229.
42. Jones, B.W., Watt, C.B., Frederick, J.M., Baehr, W., Chen, C.K., Levine, E.M., Milam, A.H., Lavail, M.M. and Marc, R.E. (2003) Retinal

remodeling triggered by photoreceptor degenerations. *J. Comp. Neurol.*, **464**, 1–16.
43. Marc, R.E. and Jones, B.W. (2003) Retinal remodeling in inherited photoreceptor degenerations. *Mol. Neurobiol.*, **28**, 139–147.
44. Rattner, A. and Nathans, J. (2005) The genomic response to retinal disease and injury: evidence for endothelin signaling from photoreceptors to glia. *J. Neurosci.*, **25**, 4540–4549.
45. Beltran, W.A., Wen, R., Acland, G.M. and Aguirre, G.D. (2007) Intravitreal injection of ciliary neurotrophic factor (CNTF) causes peripheral remodeling and does not prevent photoreceptor loss in canine RPGR mutant retina. *Exp. Eye Res.*, **84**, 753–771.
46. Avasthi, P., Watt, C.B., Williams, D.S., Le, Y.Z., Li, S., Chen, C.K., Marc, R.E., Frederick, J.M. and Baehr, W. (2009) Trafficking of membrane proteins to cone but not rod outer segments is dependent on heterotrimeric kinesin-II. *J. Neurosci.*, **29**, 14287–14298.
47. Fliegauf, M., Benzing, T. and Omran, H. (2007) When cilia go bad: cilia defects and ciliopathies. *Nat. Rev. Mol. Cell Biol.*, **8**, 880–893.
48. Roepman, R. and Wolfrum, U. (2007) Protein networks and complexes in photoreceptor cilia. *Subcell. Biochem.*, **43**, 209–235.
49. Khanna, H., Davis, E.E., Murga-Zamalloa, C.A., Estrada-Cuzcano, A., Lopez, I., den Hollander, A.I., Zonneveld, M.N., Othman, M.I., Waseem, N., Chakarova, C.F. *et al.* (2009) A common allele in RPGRIP1L is a modifier of retinal degeneration in ciliopathies. *Nat. Genet.*, **41**, 739–745.
50. Jeon, C.J., Strettoi, E. and Masland, R.H. (1998) The major cell populations of the mouse retina. *J. Neurosci.*, **18**, 8936–8946.
51. Delyfer, M.N., Léveillard, T., Mohand-Saïd, S., Hicks, D., Picaud, S. and Sahel, J.A. (2004) Inherited retinal degenerations: therapeutic prospects. *Biol. Cell.*, **96**, 261–269.
52. Chrysostomou, V., Valter, K. and Stone, J. (2009) Cone-rod dependence in the rat retina: variation with the rate of rod damage. *Invest. Ophthalmol. Vis. Sci.*, **50**, 3017–3023.
53. Zhu, X., Brown, B., Li, A., Mears, A.J., Swaroop, A. and Craft, C.M. (2003) GRK1-dependent phosphorylation of S and M opsins and their binding to cone arrestin during cone phototransduction in the mouse retina. *J. Neurosci.*, **23**, 6152–6160.
54. Farjo, R., Fliesler, S.J. and Naash, M.I. (2007) Effect of Rds abundance on cone outer segment morphogenesis, photoreceptor gene expression, and outer limiting membrane integrity. *J. Comp. Neurol.*, **504**, 619–630.
55. Feathers, K.L., Lyubarsky, A.L., Khan, N.W., Teofilo, K., Swaroop, A., Williams, D.S., Pugh, E.N. Jr and Thompson, D.A. (2008) Nrl-knockout mice deficient in Rpe65 fail to synthesize 11-cis retinal and cone outer segments. *Invest. Ophthalmol. Vis. Sci.*, **49**, 1126–1135.
56. Bramall, A.N., Wright, A.F., Jacobson, S.G. and McInnes, R.R. (2010) The genomic, biochemical, and cellular responses of the retina in inherited photoreceptor degenerations and prospects for the treatment of these disorders. *Annu. Rev. Neurosci.*, **33**, 441–472.
57. Huang, Y., Cideciyan, A.V., Papastergiou, G.I., Banin, E., Semple-Rowland, S.L., Milam, A.H. and Jacobson, S.G. (1998) Relation of optical coherence tomography to microanatomy in normal and rd chickens. *Invest. Ophthalmol. Vis. Sci.*, **39**, 2405–2416.
58. Cideciyan, A.V., Swider, M., Aleman, T.S., Roman, M.I., Sumaroka, A. and Schwartz, S.B. (2007) Reduced-illuminance autofluorescence imaging in ABCA4-associated retinal degenerations. *J. Opt. Soc. Am. A*, **24**, 1457–1467.
59. Van Hooser, J.P., Aleman, T.S., He, Y.G., Cideciyan, A.V., Kuksa, V., Pittler, S.J., Stone, E.M., Jacobson, S.G. and Palczewski, K. (2000) Rapid restoration of visual pigment and function with oral retinoid in a mouse model of childhood blindness. *Proc. Natl Acad. Sci. USA*, **97**, 8623–8628.
60. Aleman, T.S., LaVail, M.M., Montemayor, R., Ying, G., Maguire, M.M., Laties, A.M., Jacobson, S.G. and Cideciyan, A.V. (2001) Augmented rod bipolar cell function in partial receptor loss: an ERG study in P23H rhodopsin transgenic and aging normal rats. *Vision Res.*, **41**, 2779–2797.
61. Cheng, H., Aleman, T.S., Cideciyan, A.V., Khanna, R., Jacobson, S.G. and Swaroop, A. (2006) In vivo function of the orphan nuclear receptor NR2E3 in establishing photoreceptor identity during mammalian retinal development. *Hum. Mol. Genet.*, **15**, 2588–2602.